Fundamental constraints on the observability of non-Hermitian effects in passive systems

Henning Schomerus
Department of Physics, Lancaster University, Lancaster LA1 4YB, United Kingdom

(Received 16 August 2022; accepted 2 December 2022; published 19 December 2022)

Utilizing scattering theory, we quantify the consequences of physical constraints that limit the visibility of non-Hermitian effects in passive devices. The constraints arise from the fundamental requirement that the system obeys causality, and can be captured concisely in terms of an internal time-delay operator, which furthermore provides a direct quantitative measure of the visibility of specific non-Hermitian phenomena in the density of states. We illustrate the implications by contrasting two prominent non-Hermitian effects, exceptional points, and the non-Hermitian skin effect, whose underlying extreme mode nonorthogonality turns out to be undetectable in the density of states.

DOI: 10.1103/PhysRevA.106.063509

I. INTRODUCTION

Hermitian systems support orthogonal stationary modes with identical, infinite lifetimes. If the Hermiticity is of a fundamental nature, as in quantum mechanics, this plays an important role in guaranteeing the dynamical stability of the system. The situation is more complex in effectively non-Hermitian systems [1,2], for instance, photonic systems with gain or loss [3–7], where nonorthogonal modes of different lifetimes appear. These systems attract considerable attention because they can display a wide range of phenomena that can be exploited for unique applications, such as power oscillations [8–10], unidirectional transport [11] and invisibility [12], coherent absorption [13,14], mode selection [15], and lasing [16–21]. Many of these applications purposefully utilize the lifetime differences to enhance desired modes relative to undesired modes, hence achieving a clear visibility of specific modes incorporating a particular functionality by their long lifetime. Furthermore, many of these applications make explicit use of the mode nonorthogonality. Prominent examples are enhanced sensors [22–24] operating near exceptional points [25–27], which are non-Hermitian degeneracies where eigenmodes align, and directed amplifiers and sensors [28–32] facilitated by the non-Hermitian skin effect [33–37], a peculiar feature of nonreciprocal systems where bulk modes become systematically distorted towards one side.

The design of such systems has received further impetus by the realization that in non-Hermitian systems, modes with predetermined frequencies, lifetimes, and mode profiles can be protected by generalized symmetries [38–42]. This leads to rich scenarios that transcend Hermitian topological physics [43–45], both practically [46] as well as in their mathematical complexity [47–49]. However, many of these symmetries can only be realized in active systems, which incorporate components with gain that require a sustained supply of energy and introduce noise. For instance, parity-time (PT) symmetric systems with balanced gain and loss [4,5] can provide a spectrum of infinite-lifetime modes, but these are intrinsically destabilized by the quantum noise in the active regions [50–52]. Furthermore, present experimental realizations of the non-Hermitian skin effect [53–57] all invoke active elements. Analogously, noise limits the precision of exceptional-point sensors [58], and nonadiabatic transients from lifetime differences limit the observability of the half-integer Berry phase of these points [59,60]. Even in the passive setting, many of the most coveted non-Hermitian effects can be made visible only with specially tailored excitations. In view of these challenges, it is highly desirable to base non-Hermitian functionality on the generic scattering response of passive stationary devices, which is encoded in the density of states.

In this work, we establish and evaluate a stringent fundamental constraint on this objective, which arises from the requirement that the underlying microscopic physics obeys causality [61]. This requirement is stronger than just insisting on the dynamical stability of the modes in the system (hence, on nonnegative lifetimes), and takes care of the fact that the system is not isolated, but couples to the components supplying the loss. However, the constraints can be readily formulated in general terms and evaluated quantitatively in given systems. From this we can determine general limits of the visibility of specific non-Hermitian effects.

To establish these links systematically, we first formulate the constraints compactly by phrasing them in terms of the language of scattering theory (Sec. II). Causality is then encoded into the internal time-delay operator, a central object from scattering theory that can be obtained from the microscopic model. From this, one can obtain the critical threshold value of overall losses that a model necessarily needs to include to be realizable in a passive device. These conditions can be classified by symmetries inherited from the effective Hamiltonian, which establishes a systematic link between non-Hermitian and Hermitian symmetry classes (Sec. III). To evaluate the consequences in practical settings (Sec. IV), we exploit that the time-delay operator directly determines the experimentally observed density of states, which serves

as a quantitative measure of the visibility of specific non-Hermitian effects. We apply this to scenarios of particular theoretical and experimental interest, comprising systems displaying exceptional points, the non-Hermitian skin effect, and edge states. Remarkably, in the passive setting, the extreme mode nonorthogonality underlying exceptional points and the skin effect cannot be detected from the density of states. As we describe in the conclusions (Sec. V), the results presented here invite attention to revisit the physical interpretation of mathematical features and classifications of non-Hermitian systems. Appendices provide further background on the scattering formalism, symmetry classification, and numerical results backing up these conclusions.

II. GENERAL FORMULATION OF CAUSALITY CONSTRAINTS

For concreteness, we base the considerations on coupled-mode theory, which enjoys a wide range of applications from photonic to mechanical systems and mimics the language of quantum mechanics. In this theory, one employs a basis corresponding to a suitable set of bare modes, often identified with individual components such as resonators or waveguides, and collects their intrinsic properties and couplings in a matrix H that serves as an effective Hamiltonian. We assume that the elements of H are frequency independent, but note that effects of additional frequency dispersion can be accounted for by including auxiliary components [62]. This effective Hamiltonian serves as the input to model and design experiments, and also is the ubiquitous starting point for theoretical considerations, such as about the role of symmetries in these systems, as specified further below. For the moment, the key feature of the effective Hamiltonian is that it can be non-Hermitian, $H \neq H^\dagger$. On the basis of the microscopic model, we capture this quantitatively by writing the Hamiltonian in the form

$$H = H_0 + iF - i\gamma, \tag{1}$$

which separates out the Hermitian parts $H_0 = H_0^\dagger$, nontrivial anti-Hermitian parts with $iF = -(iF)^\dagger$, as well as an overall level of uniform scalar background losses γ, which is determined by requiring $\mathrm{tr}\, F = 0$. As we describe further below, the operator F governs the desired non-Hermitian symmetries and effects, which then become realizable in a passive device when γ exceeds a certain threshold value γ_c.

To identify this threshold and establish the ensuing limits on the visibility of non-Hermitian effects on physical grounds, we adopt a common measurement protocol of the density of states and probe the system from the outside to detect its resonant response. Let us assume that the system is uniformly coupled to the outside at a coupling strength Γ. In the wide-band limit, where all spectral features in the scattered signal are due to the system, the scattering matrix is given by [63–66]

$$S(\omega) = [1 - i\Gamma\mathcal{G}(\omega)][1 + i\Gamma\mathcal{G}(\omega)]^{-1}, \tag{2}$$

where $\mathcal{G}(\omega) = (\omega - H_0 - iF + i\gamma)^{-1}$ is the Greens function of the system (see Appendix A for background of this formalism). From the scattering perspective, the system is passively realizable if it does not amplify any incoming signal $\mathbf{a}$, i.e., if $||S\mathbf{a}|| \leqslant ||\mathbf{a}||$, irrespective of whether the incoming signal is designed to couple into a specific mode or not. This means that the operator combination $S^\dagger S$ has no eigenvalues exceeding 1, or equivalently, that the expression $1 - S^\dagger S$ is positive semidefinite. With Eq. (2), this condition can be reformulated instructively by writing

$$1 - S^\dagger S = 2\Gamma Q_\Gamma, \tag{3}$$

where

$$Q_\Gamma = 2[\mathcal{G}(\omega + i\Gamma)]^\dagger(\gamma - F)\mathcal{G}(\omega + i\Gamma) \tag{4}$$

is the celebrated time-delay operator [66–69], recovering it in a form that remains valid in a non-Hermitian system [70]. Via Eq. (3), its elements can be directly determined in experiments from the scattering strength. For a passively realizable system we then have to demand that Q_Γ is positive semidefinite.

This formulation is useful because it provides a unifying perspective on different aspects of the system.

Firstly, it confirms that on the simplest level, a microscopic model can be physically realized in a passive system when the combination $\gamma - F$ itself is positive semidefinite [71], hence if γ is larger than the largest eigenvalue of F. We denote the eigenvalues of F as f_k, so that $\gamma_c = \max f_k$. This constraint is both *simpler* and *stronger* than requiring positive lifetimes τ_k of all modes, which are encoded in the eigenvalues $\Omega_k = \omega_k - i/2\tau_k$ of the effective Hamiltonian H itself, and related mathematical constraints such as the Lee-Wolfenstein and Bell-Steinberger relations [71–73].

Secondly, the positive semidefiniteness of the delay times guarantees causality of the system, which clarifies the fundamental physical nature of the constraint, and justifies to call γ_c the *causality threshold*.

Thirdly, the time-delay operator delivers a direct measure of the generic visibility of physical effects, the density of states $\rho(\omega) = (2\pi)^{-1}\,\mathrm{tr}\, Q_\Gamma(\omega)$, which accounts for the mode broadening by the intrinsic and radiative losses, and via Eq. (3) is directly accessible from the experimental scattering signal [65,69]. We read off that for fixed H_0 and F, the passive visibility of individual modes in this measure is maximized for $\Gamma = 0$ and $\gamma = \gamma_c$, hence at the causality threshold of a weakly probed system. Below, we will use this measure to quantify the properties of specific systems from different symmetry classes, whose general features we describe next.

III. EVALUATION IN SPECIFIC SYMMETRY CLASSES

Effectively non-Hermitian Hamiltonians appear in many guises, and the physical symmetries of a system translate into different mathematical forms that reflect the context. For example, the effective Hamiltonian may generate the time evolution of a wave function in a slowly varying envelope coupled-mode description, which is analogous to the Schrödinger equation, it may feature in the propagation of a density matrix, or it may appear in a stability analysis or Bogoliubov theory that includes complex-conjugated fields [39,40,42]. In the identification of the causality constraints above, we adopted the language of scattering theory, and we therefore apply the corresponding notions when identifying the symmetries of the system [45,74,75]. Specifically, conventional time-reversal (T) symmetry then entails $H = H^*$, and in a reciprocal system we have $H = H^T$ (we will refer

to this as the T' symmetry). Furthermore, PT symmetry dictates $\mathcal{X}H\mathcal{X} = H^*$, and a non-Hermitian charge-conjugation (C) symmetry entails $\mathcal{X}H\mathcal{X} = -H^*$, involving in each case a suitable unitary operator fulfilling $\mathcal{X}^2 = 1$. We will also consider variants of these systems with $\mathcal{X}H\mathcal{X} = H^\dagger$ (PTT') and $\mathcal{X}H\mathcal{X} = -H^\dagger$ (CT'), which constitute separate symmetry classes when the system is nonreciprocal.

It should be noted that several of these symmetries can only be realized for $\gamma = 0$. To extend them to the passive setting, we hence assume that they hold for $H = H_0 + iF$, and then consider the same model at finite γ, following the established example of passive PT symmetry [9]. The symmetry can then be realized passively for $\gamma \geqslant \gamma_c$. These symmetries can be combined in different ways, leading to an extensive classification [39,40], where the cases above are of particular theoretical and experimental interest. For instance, nonreciprocal systems with $H = H^* \neq H^T$ are the simplest setting in which the non-Hermitian skin effect appears.

Before we address the visibility of such effects, let us examine the general structure of the causality constraints in these symmetry classes. We express this compactly in terms of the symmetries inherited by the operator F capturing the nontrivial non-Hermitian content of the model, and refer to Appendix B for a detailed description in terms of the block structure of this operator.

We start with the case of a PT-symmetric system. From the definition of the symmetry in terms of the effective Hamiltonian, we see that the operator F then obeys a Hermitian charge-conjugation symmetry, $\mathcal{X}F\mathcal{X} = -F^*$, as encountered in a superconductor [45]. This enforces a symmetry of its spectrum, with eigenvalues appearing in pairs $\pm|f_k|$. For a PTT' symmetry, the operator F displays a chiral symmetry, $\mathcal{X}F\mathcal{X} = -F$, again leading to a spectral symmetry of its eigenvalues. Both variants coincide if the system is reciprocal, $H = H^T$, where F is real and obeys time-reversal symmetry.

For systems with a C symmetry, $F = \mathcal{X}F^*\mathcal{X}$ displays a generalized time-reversal symmetry, while CT' entails that $F = \mathcal{X}F\mathcal{X}$ obeys a unitary symmetry, and hence can be block-diagonalized into the symmetry sectors of $\mathcal{X}$. Finally, in a nonreciprocal system with passive T symmetry, $F = -F^T$, as is typical for a topologically nontrivial superconductor in the so-called Majorana basis [45]. In all cases, we see that there is a systematic link from a non-Hermitian symmetry class to a Hermitian symmetry class.

This concludes our first main objective of formulating a convenient general framework for the causality constraints. We now apply it to quantify the visibility of non-Hermitian effects in concrete settings.

IV. OBSERVABILITY OF SPECIFIC NON-HERMITIAN EFFECTS

As mentioned in the introduction, exceptional points (from here on EPs), where eigenvalues collide in the complex plane and eigenmodes align, are one of the most prominent features of non-Hermitian systems. Their effects are most easily seen for modes of long lifetimes, such as in active photonic systems near the laser threshold [16–19], which then are highly sensitive to perturbations [22–24]. The enhanced sensitivity also applies to the noise from spontaneous emission and response to external driving, which at the EP results in an unconventional *squared-Lorentzian* line shape [51,76–79]. This celebrated result has been originally derived in the input-output scattering formalisms of active systems [80,81], which analyzes $S^\dagger S - 1$, and shows that the modified line shape is linked to the drastic violation of mode orthogonality at the EP.

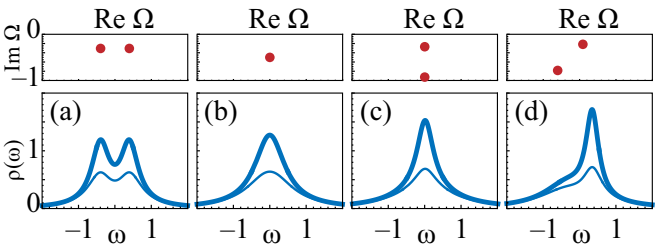

FIG. 1. Complex eigenvalue spectrum Ω_k (top) and density of states $\rho(\omega)$ (bottom) for the effective Hamiltonian (5). The couplings are fixed to $b = c^* = 0.4 - 0.3i$, while (a) $a = \sqrt{-bc} - 0.2i$ (PT symmetric case), (b) $a = \sqrt{-bc}$ (EP), (c) $a = \sqrt{-bc} + 0.1i$ (dynamically broken phase), and (d) $a = \sqrt{-bc} + 0.2$ (symmetry explicitly broken). The thick lines are for the limit of weak couplings $\Gamma = 0$, where the lifetimes are maximized. At the exceptional point, $\rho(\omega)$ is then a simple Lorentzian, which does not reveal the extreme mode nonorthogonality of the system. The thin lines are for finite $\Gamma = 0.1$, where a squared-Lorentzian background of limited contrast appears at the EP.

To assess the observability of these features in the density of states of passive systems, we adopt the standard reduced 2×2 Hamiltonian

$$H = \begin{pmatrix} a - i\gamma & b \\ c & -a - i\gamma \end{pmatrix}, \tag{5}$$

where we initially allow for the most general case with complex parameters a, b, and c. The causality constraint then follows from the matrix

$$F = (-i/2)\begin{pmatrix} a - a^* & b - c^* \\ c - b^* & -a + a^* \end{pmatrix}, \tag{6}$$

giving the threshold value $\gamma_c = \sqrt{(\mathrm{Im}\, a)^2 + |b - c^*|^2/4}$.

In Fig. 1 we show the threshold density of states $\rho(\omega)$ for different scenarios at and away from the EP, which occurs for $a^2 + bc = 0$. In the figure, the EP signals a spontaneous symmetry-breaking transition, where the eigenvalue pair moves away from the spectral symmetry line $\mathrm{Im}\,\omega = -\gamma$. At the EP, this density of states is given by

$$\rho^{(\mathrm{EP})}(\omega) = \frac{1}{\pi} \frac{|b| + |c|}{\omega^2 + (|b| + |c|)^2/4}. \tag{7}$$

This is a *simple* Lorentzian normalized to 2, and hence accounts for both states in the same way as in a Hermitian system with orthogonal states, irrespective of the actual extreme mode nonorthogonality at the degeneracy. A squared-Lorentzian background of limited contrast only appears at finite coupling Γ (dashed lines). However, this background comes with a negative spectral weight that never exceeds $1/4$ of the Lorentz contribution (see Appendix C), with the optimal contrast attained at $\Gamma \sim \gamma_c$ where the density of states is

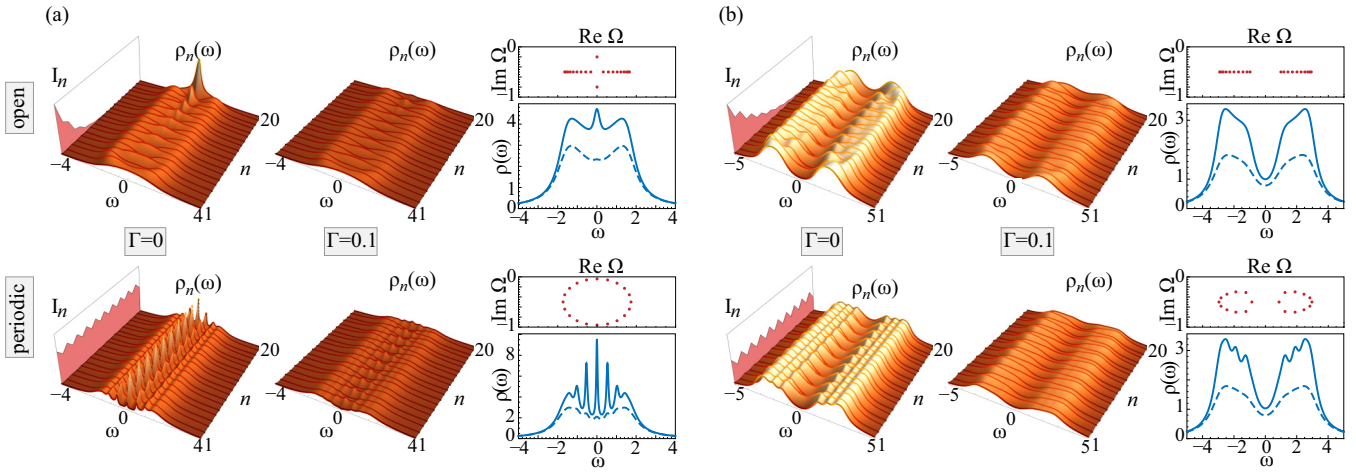

FIG. 2. Absent signatures of the non-Hermitian skin effect in the local and global density of states $\rho_n(\omega)$ and $\rho(\omega)$, illustrated for systems of 20 sites with open (top) and periodic (bottom) boundary conditions at weak coupling $\Gamma \to 0$ (left subpanels/solid curves) and moderate coupling $\Gamma = 0.1$ (right subpanels/dashed curves). The system is modeled by Eq. (8) with $v_1 = -0.8i$, $v_2 = -0.2i$, $u_1^{\pm} = \bar{u} \mp 0.4$, $u_2^{\pm} = 1$, $w = 0$, and (a) $\bar{u} = 0.8$, (b) $\bar{u} = 2$. The physical density of states is compared to the mathematical summed eigenvector profile I_n displaying the skin effect, and the complex eigenvalues Ω of H.

already strongly suppressed due to the much reduced lifetime to the states.

In other symmetry classes, functionality can arise collectively from the bulk, or individually from particular states. To determine their visibility we consider a flexible one-dimensional model encompassing a wide range of paradigms [34,38,82–89], based on an effective Hamiltonian

$$H_{nm} = \delta_{n,m} v_n + \delta_{n,m-1} u_n^- + \delta_{n,m+1} u_m^+ + \delta_{n,m-2} w_n + \delta_{n-2,m} w_m. \tag{8}$$

The imaginary parts of the complex on-site potentials v_n induce distributed losses, while the real parts allow to define a corrugated potential. The couplings $u_n^{\pm}$ can be arranged to induce zero modes, and when they are nonreciprocal they induce the non-Hermitian skin effect. For the moment, we also include reciprocal real next-nearest-neighbor couplings w_n as they allow to obtain the skin effect from scalar losses and real magnetic fields [84] and feature in some experiments [53].

All these effects appear in a periodic dimer arrangement with a two-site unit cell, which induces a nontrivial band structure governed by the Bloch Hamiltonian

$$H(k) = \begin{pmatrix} v_1 + 2w_1 \cos k & u_1^- + u_2^+ e^{-ik} \\ u_1^+ + u_2^- e^{ik} & v_2 + 2w_2 \cos k \end{pmatrix}. \tag{9}$$

With conventional periodic boundary conditions, k is real, but to fulfill the open boundary conditions of a finite system one generically needs to combine spectrally degenerate nonreciprocal modes with complex k [90–92]. Hence, the modes display an exponential spatial profile distorted toward the edge, which is the essence of the non-Hermitian skin effect. In the Hermitian limit, these modes become conventional extended Bloch states, with the possible exception of a finite number of edge states that maintain an exponentially decaying profile. This complex interplay of effects explains why the non-Hermitian skin effect has received considerable attention.

In contrast, the causality constraints on the bulk and edge modes are governed much more simply by the Bloch version of the operator F,

$$F(k) = \begin{pmatrix} \Delta v & \Delta u_1^* + \Delta u_2 e^{-ik} \\ \Delta u_1 + \Delta u_2^* e^{ik} & -\Delta v \end{pmatrix}, \tag{10}$$

where $\Delta v = \mathrm{Im}\,(v_1 - v_2)/2$ and $\Delta u_n = -i(u_n^+ - u_n^{-*})/2$. This is a standard Hermitian dimer chain with two symmetric bands, encompassing the Su-Schrieffer Heeger [93] and Rice-Mele [94] models as special cases. These models can support edge states, but they occur in the middle of the spectrum, while we are interested in the upper edge of the spectrum. Furthermore, being Hermitian, F does not suffer from any complications of the skin effect, so that this upper edge can be found from the Bloch version. Therefore, in large systems the causality threshold

$$\gamma_c = \sqrt{(\Delta v)^2 + (|\Delta u_1| + |\Delta u_2|)^2} \tag{11}$$

coincides for both types of boundary conditions, and hence is also insensitive to the skin effect.

To assess how visible these effects are in the passive setting, we use the spatially resolved density of states $\rho_n = Q_{nn}/2\pi$, again evaluated to the causality threshold. Figure 2 illustrates this in different scenarios (see Appendix D for further numerical results). The top row shows results for a finite system with open boundary conditions, where each panel further contrasts weak and strong coupling Γ. In panel (a), the system supports an edge state, which for $\Gamma = 0$ is clearly visible in the local and total density of states, while no such edge state exists in panel (b). In both panels, the eigenstates display the non-Hermitian skin effect, as quantified by the summed profile $I_n \equiv (UU^\dagger)_{nn}$ of normalized eigenvectors, collected in the diagonalizing matrix U. However, this effect is completely absent in the density of states, to the extent that it does not even appear as a background effect at finite Γ. Indeed, the spatial profile of the bulk density of states is similar to that in a system with periodic boundary conditions (bottom row), even though the eigenfunctions and eigenvalue spectra of both cases dramatically differ.

V. CONCLUSIONS

In summary, we have established general constraints on the observability of non-Hermitian effects in passive devices, and evaluated the implications for prominent paradigms, including exceptional points, the non-Hermitian skin effect, and symmetry-protected edge states. Some of the most widely sought-after features, in particular the signatures of drastic mode nonorthogonality, cannot be detected in the density of states. These findings highlight the essential role of active elements in devices that aim to exploit these signatures, which generally suffer from other complications such as unavoidable material dispersion.

Being formulated in a unifying scattering approach, the general results apply to various platforms, such as photonic, mechanical, and acoustic systems, electronic circuits, or microwave networks, and can be readily used to quantify the visibility of effects in a wide range of models. This also provides guidance for the design of passive devices in which the visibility is maximized, and allows to discard designs relying on effects whose observability is severely limited.

More broadly, the results presented here imply that the physics of passive non-Hermitian systems is not governed just by the mathematical symmetry class of their effective Hamiltonian [39,40,42], but is also systematically linked to an operator from a specific Hermitian symmetry class, which can display its own distinct phases and transitions—features that are not included in the existing classifications. For instance, there is a clear physical distinction between settings where a non-Hermitian spectral symmetry applies with respect to the real axis or the imaginary axis of the complex frequency plane. This realization introduces additional richness into the physical properties of these systems, whose role can also be explored in active and nonlinear settings, in particular when considering their quantum-limited sensitivity to noise.

ACKNOWLEDGMENTS

I gratefully thank Jan Wiersig for very useful discussions, and Franco Nori and his group for generous hospitality at RIKEN during the latter stages of this work. This work was partially funded by the Japanese Society for the Promotion of Science via JSPS invitational Fellowship No. L20556.

APPENDIX A: DETAILS OF THE DERIVATION OF GENERAL EXPRESSIONS

The scattering matrix given in Eq. (2) can be derived in several standard formalisms, see Refs. [63–66], which also cover a range of applications and extensions. Here, we present an explicit derivation in the instructive physical setting where each internal site is coupled with a strength Γ to a dedicated single-channel waveguide (from the formal steps, this physical derivation corresponds closely to the mathematical one given in the introduction of Ref. [66]). We denote the real-space components inside the system by $\psi_{\rm int}$, and the incoming and outgoing traveling-wave components in the waveguides by $a_{\rm in}$, $a_{\rm out}$. This scenario then translates into the wave-matching equations

$$(\omega - H)\psi_{\rm int} = \Gamma(a_{\rm out} + a_{\rm in}) \tag{A1}$$

(matching the wave functions) and

$$\psi_{\rm int} = i a_{\rm out} - i a_{\rm in} \tag{A2}$$

(matching their derivatives in a manifestly flux-conserving form). We multiply the second of these two equations by $\pm i\Gamma$ and add the result to the first equation, so that

$$(\omega - H + i\Gamma)\psi_{\rm int} = 2\Gamma a_{\rm in}, \tag{A3}$$

$$(\omega - H - i\Gamma)\psi_{\rm int} = 2\Gamma a_{\rm out}. \tag{A4}$$

Therefore,

$$a_{\rm out} = (\omega - H - i\Gamma)(\omega - H + i\Gamma)^{-1} a_{\rm in} \equiv S a_{\rm in}. \tag{A5}$$

From this we directly read off S, which in Eq. (2) is conveniently written in terms of the internal Green's function, $\mathcal{G}(\omega) = (\omega - H)^{-1}$.

In experiments, the density of states can be inferred from this setup by analyzing the losses into the system [65]. This is formalized by the left-hand side of Eq. (3), while theoretically the link is established using the relation to the underlying Greens function [69]. The right-hand side then follows directly by inserting the scattering matrix into this expression,

$$\begin{aligned} 1 &- (\omega - H^\dagger - i\Gamma)^{-1}(\omega - H^\dagger + i\Gamma)(\omega - H - i\Gamma) \\ &\times(\omega - H + i\Gamma)^{-1} \qquad\qquad (A6)\\ &= (\omega - H^\dagger - i\Gamma)^{-1}[(\omega - H^\dagger - i\Gamma)(\omega - H + i\Gamma) \\ &\quad -(\omega - H^\dagger + i\Gamma)(\omega - H - i\Gamma)](\omega - H + i\Gamma)^{-1} \qquad (A7)\\ &= 2\Gamma(\omega - H^\dagger - i\Gamma)^{-1}[i(H - H^\dagger)](\omega - H + i\Gamma)^{-1} \\ &\equiv 2\Gamma Q_\Gamma, \qquad\qquad (A8) \end{aligned}$$

where we then identify $(\omega - H + i\Gamma)^{-1} = \mathcal{G}(\omega + i\Gamma)$ and $i(H - H^\dagger) = 2(\gamma - F)$.

The resulting combination Q_Γ of Greens functions is precisely the time-delay operator [66,69], written in a form that remains valid in non-Hermitian systems [70]. We note that in Hermitian systems, where the scattering matrix S is unitary, the time-delay operator can also be written as $Q = -iS^\dagger dS/d\omega$, as it was indeed introduced originally by Wigner and Smith [67,68].

APPENDIX B: CONCRETE FORMS OF THE SYMMETRIES OF THE NONTRIVIAL NON-HERMITIAN CONTENT *F*

In Sec. III, we identified the symmetries inherited by the operator F in general terms. Here, we express these symmetries concretely in terms of the block structure of this operator. We again start with the case of a PT-symmetric system. Taking $\mathcal{X}$ of the form of a Pauli-x block matrix, as commonly done to reflect the physical design with symmetrically placed balanced gain and loss components, the effective Hamiltonian is of the form

$$H = \begin{pmatrix} A - i\gamma & B \\ B^* & A^* - i\gamma \end{pmatrix} \tag{B1}$$

with general subblocks A and B. The nontrivial non-Hermitian content is captured by the operator

$$F = \frac{-i}{2}\begin{pmatrix} A - A^\dagger & B - B^T \\ B^* - B^\dagger & A^* - A^T \end{pmatrix}. \tag{B2}$$

This displays the symmetries of a superconductor with a Hermitian charge-conjugation symmetry, $\mathcal{X}F\mathcal{X} = -F^*$, and enforces the symmetry of its spectrum, with eigenvalues paired as $\pm|f_k|$.

For a PTT' symmetry,

$$H = \begin{pmatrix} A - i\gamma & B \\ C & A^\dagger - i\gamma \end{pmatrix}, \tag{B3}$$

where $B = B^\dagger$ and $C = C^\dagger$. Therefore,

$$F = \frac{-i}{2}\begin{pmatrix} A - A^\dagger & B - C \\ C - B & A^\dagger - A \end{pmatrix} \tag{B4}$$

now displays a chiral symmetry, $\mathcal{X}F\mathcal{X} = -F$, again leading to a spectral symmetry of its eigenvalues. The block structures of the PT and PT' variants coincide if the system is reciprocal, $H = H^T$, where F is real and obeys time-reversal symmetry.

For systems with a C symmetry, one conventionally chooses $\mathcal{X}$ of the form of a Pauli-z block matrix, as this allows for cases with a nontrivial topological index $\nu = \mathrm{tr}\,\mathcal{X}$. The effective Hamiltonian then has the structure

$$H = \begin{pmatrix} iA - i\gamma & B \\ C & iD - i\gamma \end{pmatrix}, \tag{B5}$$

with real matrices A, B, C, D, and γ chosen such that $\mathrm{tr}(A + D) = 0$. This entails that

$$F = \frac{-i}{2}\begin{pmatrix} i(A + A^T) & B - C^T \\ C - B^T & i(D + D^T) \end{pmatrix} = \mathcal{X}F^*\mathcal{X} \tag{B6}$$

displays a generalized time-reversal symmetry.

Analogously, for a system with CT' symmetry,

$$H = \begin{pmatrix} iA - i\gamma & B \\ B^\dagger & iD - i\gamma \end{pmatrix}, \tag{B7}$$

with general B and Hermitian A and D, once more obeying $\mathrm{tr}(A + D) = 0$. This entails that

$$F = \begin{pmatrix} A & 0 \\ 0 & D \end{pmatrix} = \mathcal{X}F\mathcal{X} \tag{B8}$$

is indeed block-diagonalized into the symmetry sectors of $\mathcal{X}$.

Finally, in a nonreciprocal system with passive T symmetry,

$$H = \begin{pmatrix} A - i\gamma & B \\ C & D - i\gamma \end{pmatrix}, \tag{B9}$$

with real blocks A, B, C, D, and

$$F = (-i/2)\begin{pmatrix} A - A^T & B - C^T \\ C - B^T & D - D^T \end{pmatrix} = -F^T, \tag{B10}$$

which indeed coincides with the block structure of the Hamiltonian for a topologically nontrivial superconductor in the Majorana basis.

APPENDIX C: ANALYTICAL DISCUSSION OF THE VISIBILITY OF EXCEPTIONAL POINTS

Here, we provide further analytical details for the signatures of mode nonorthogonality in the density of states near an exceptional point, as obtained from the model Hamiltonian Eq. (5). From the definitions, this density of states can be written analytically as

$$\begin{aligned}\rho(\omega) = {} & \frac{2\mathrm{Re}\,[(a^2 + bc)(\gamma + \Gamma + i\omega)]}{\pi|a^2 + bc + (\gamma + \Gamma + i\omega)^2|^2} \\ & + \frac{2\gamma|\gamma + \Gamma + i\omega|^2}{\pi|a^2 + bc + (\gamma + \Gamma + i\omega)^2|^2} \\ & - \frac{\Gamma(2|a|^2 + |b|^2 + |c|^2)}{\pi|a^2 + bc + (\gamma + \Gamma + i\omega)^2|^2}.\end{aligned} \tag{C1}$$

At the exceptional point $a^2 + bc = 0$, this reduces to

$$\rho^{(\mathrm{EP})}(\omega) = \rho^{(1)}(\omega) + \rho^{(2)}(\omega), \tag{C2}$$

$$\rho^{(1)}(\omega) = \frac{2\gamma}{\pi|\gamma + \Gamma + i\omega|^2}, \tag{C3}$$

$$\rho^{(2)}(\omega) = -\frac{\Gamma(|b| + |c|)^2}{\pi|\gamma + \Gamma + i\omega|^4}, \tag{C4}$$

hence, the sum of a simple Lorentzian and a squared Lorentzian, where the latter one only appears for finite Γ. Equation (6) is obtained for $\Gamma = 0$, $\gamma = \gamma_c = (|b| + |c|)/2$, where the width $\gamma + \Gamma$ of the simple Lorentzian is minimized in a passive system, and its weight

$$S_1(\Gamma) = \int_{-\infty}^{\infty} \rho^{(1)}(\omega)d\omega = \frac{2\gamma}{\gamma + \Gamma} \tag{C5}$$

is maximized.

The squared Lorentzian carries a negative weight

$$S_2(\Gamma) = \int_{-\infty}^{\infty} \rho^{(2)}(\omega)d\omega = -\frac{\Gamma(|b| + |c|)^2}{2(\gamma + \Gamma)^3}. \tag{C6}$$

Therefore, using again $\gamma \geqslant \gamma_c = (|b| + |c|)/2$, in a passive system the relative weight

$$\frac{|S_2(\Gamma)|}{S_1(\Gamma)} = \frac{\Gamma(|b| + |c|)^2}{4\gamma(\gamma + \Gamma)^2} \leqslant \frac{\Gamma\gamma}{(\gamma + \Gamma)^2} \leqslant \frac{1}{4}, \tag{C7}$$

where the maximum is attained at $\gamma = \Gamma = \gamma_c$.

Following the same steps, we can also compare the relative peak heights of these two contributions,

$$\frac{|\rho^{(2)}(0)|}{\rho^{(1)}(0)} = \frac{\Gamma(|b| + |c|)^2}{2\gamma(\gamma + \Gamma)^2} \leqslant \frac{1}{2}, \tag{C8}$$

which again is maximized at $\gamma = \Gamma = \gamma_c$. We note that the density of states formally turns negative for $\gamma < \gamma_c/\sqrt{2}$, which is less stringent than the causality constraint.

APPENDIX D: ADDITIONAL NUMERICAL RESULTS

In Sec. IV we showed numerical results for particularly interesting scenarios in which the underlying non-Hermitian effects are realized cleanly. To illustrate the general nature of our findings, we show in Fig. 3 additional results for the EP model (5), evaluated at parameters where PT and PTT' symmetries are manifestly broken also by the couplings. Analogously, we show additional results for the non-Hermitian skin effect, covering the case where some bulk states in the

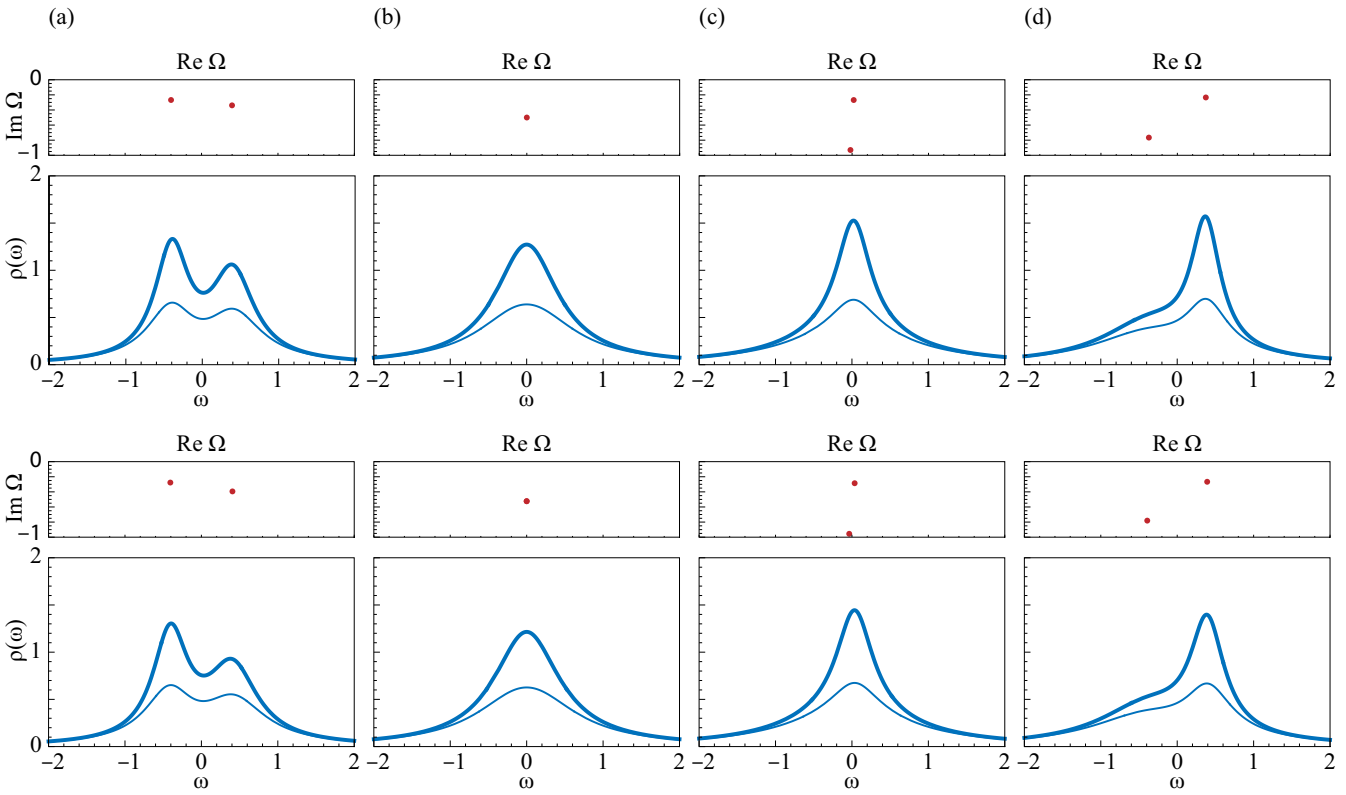

FIG. 3. Analogous to Fig. 1, but with complex nonreciprocal coupling parameters $b = 0.3 - 0.4i$, $c = 0.4 + 0.3i$ (top) $b = 0.6$, $c = 0.4 - 0.2i$, while again (a) $a = \sqrt{-bc} - 0.2i$, (b) $a = \sqrt{-bc}$ (EP), (c) $a = \sqrt{-bc} + 0.1i$, and (d) $a = \sqrt{-bc} + 0.2$. At the exceptional point, $\rho(\omega)$ is again a simple Lorentzian.

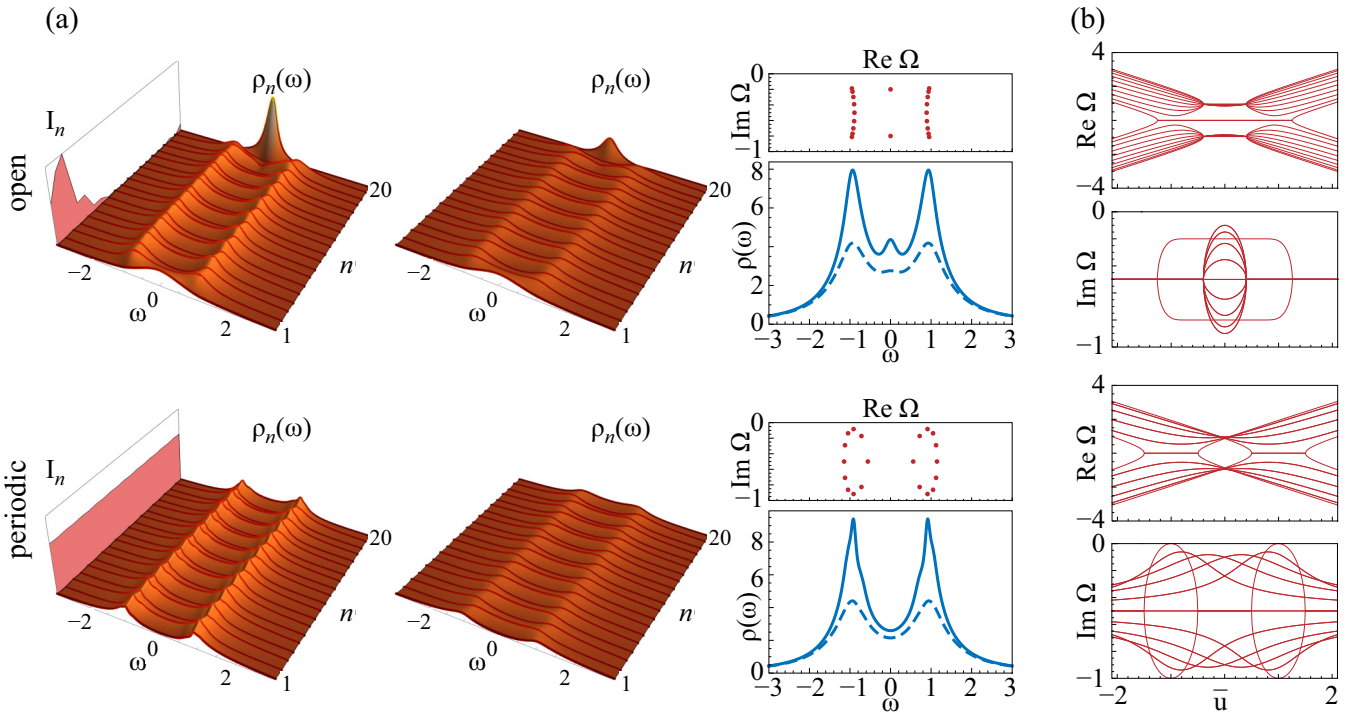

FIG. 4. (a) Analogous to Fig. 2, but for $\bar{u} = 0.25$, where the bulk modes in the system with open boundary conditions have moved away from the symmetry line in the complex frequency plane. (b) Evolution of the eigenvalues with the parameter $\bar{u}$.

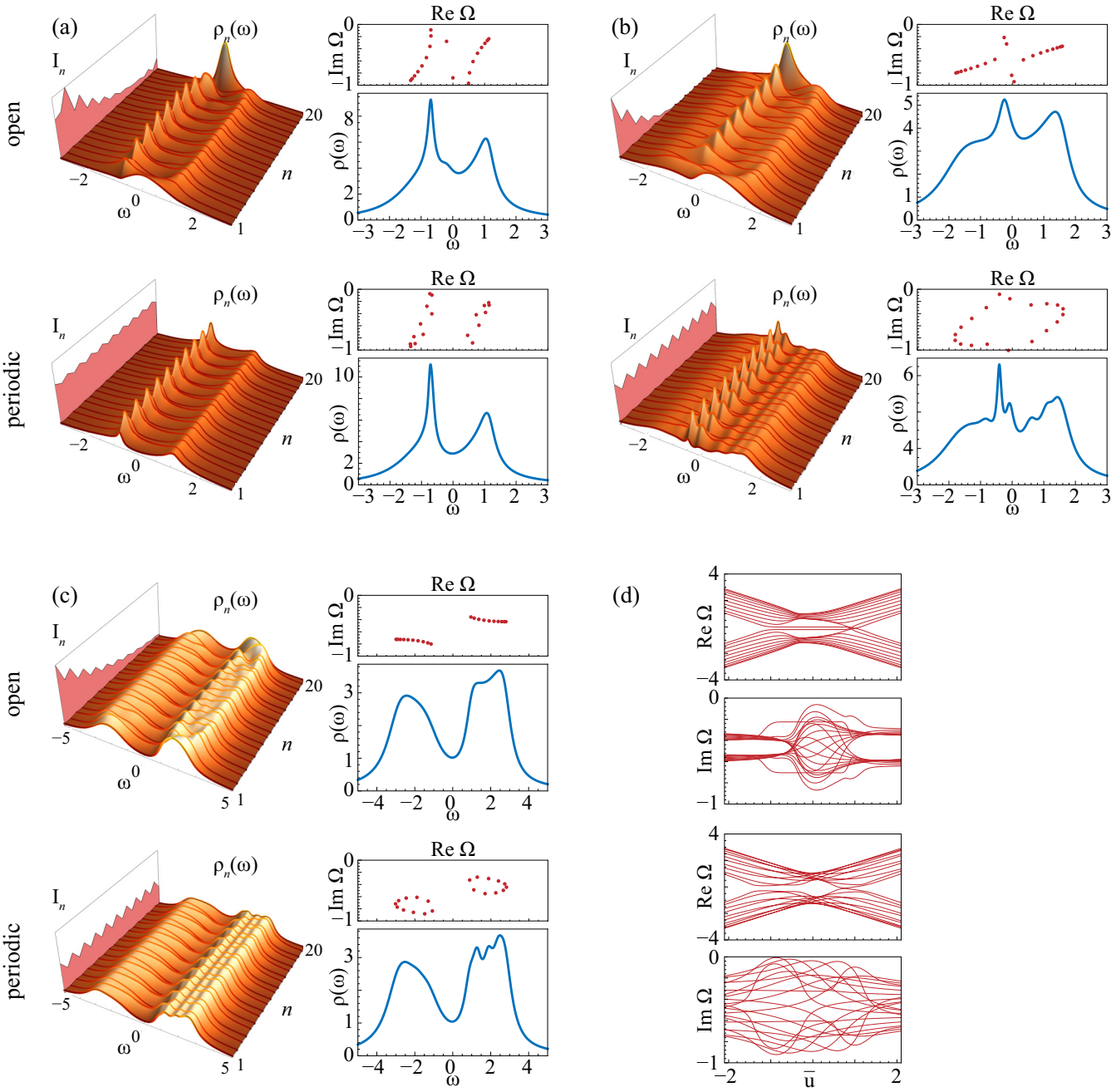

FIG. 5. Analogous to Figs. 2 and 4, but for $\Gamma = 0$ only, and the other parameters set to $v_1 = -0.3i - i\gamma_c$, $v_2 = -0.2 + 0.3i - i\gamma_c$, $u_1^+ = \bar{u} - 0.4 + 0.4i$, $u_1^- = \bar{u} + 0.4 - 0.1i$, $u_2^+ = 1 - 0.1i$, $u_2^- = 0.9$, $w_1 = w_2 = 0$, and (a) $\bar{u} = 0.25$, (b) $\bar{u} = 0.8$, (c) $\bar{u} = 2$. Panel (d) shows the evolution of the eigenvalues with the parameter $\bar{u}$.

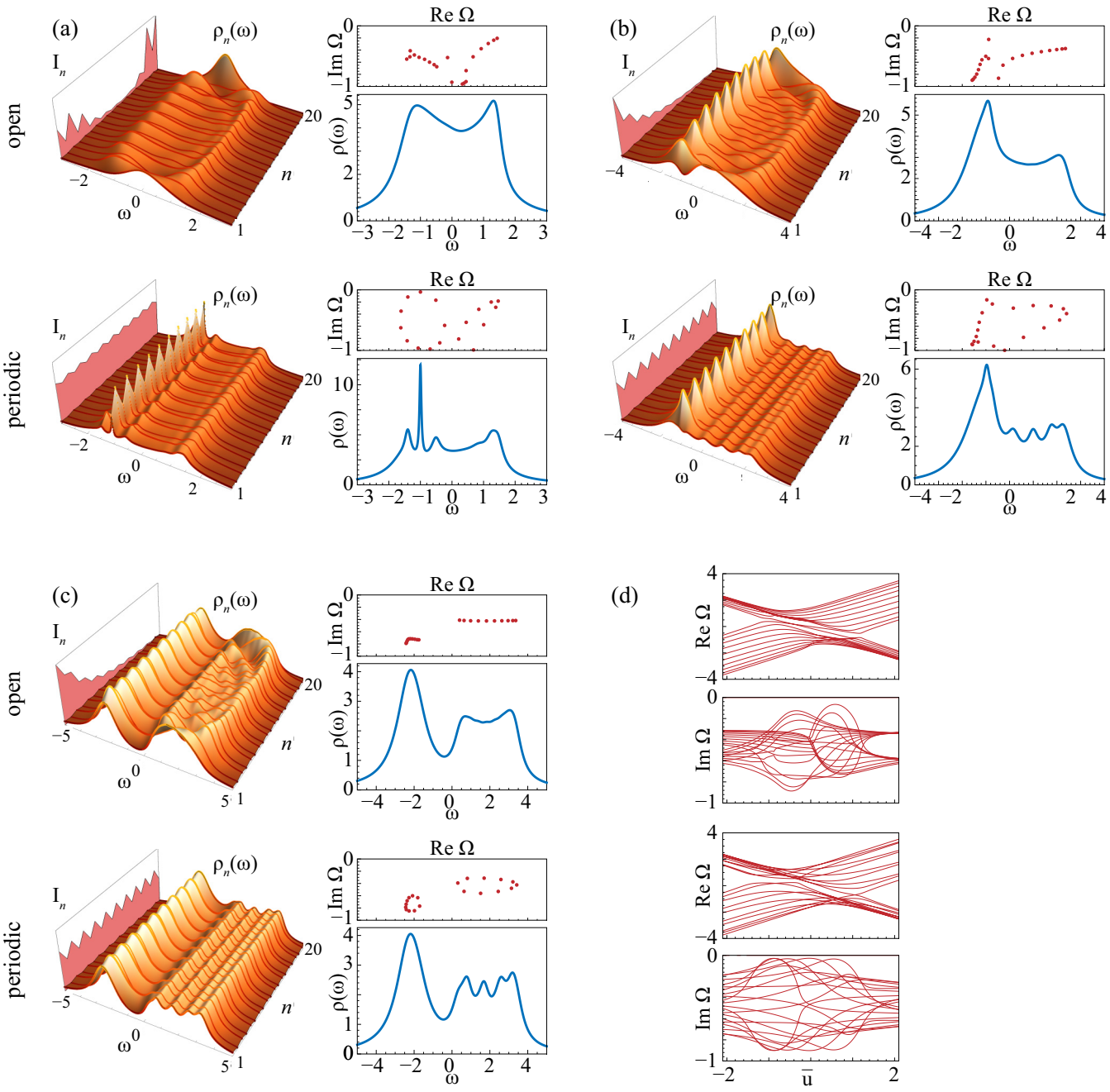

FIG. 6. Analogous to Fig. 5, but including next-nearest-neighbor couplings $w_1 = 0.2$, $w_2 = 0.4$, while here (a) $\bar{u} = 0$, (b) $\bar{u} = 1$, (c) $\bar{u} = 2$.

open system have moved away from the symmetry line in the complex plane (Fig. 4), as well as parameter configurations in which all spectral symmetries are explicitly broken (Fig. 5), including by next-nearest-neighbor couplings (Fig. 6).

[1] N. Moiseyev, *Non-Hermitian quantum mechanics* (Cambridge University Press, Cambridge, 2011)

[2] Y. Ashida, Z. Gong, and M. Ueda, Non-Hermitian physics, Adv. Phys. **69**, 249 (2020).

[3] H. Cao and J. Wiersig, Dielectric microcavities: Model systems for wave chaos and non-Hermitian physics, Rev. Mod. Phys. **87**, 61 (2015).

[4] L. Feng, R. El-Ganainy, and L. Ge, Non-Hermitian photonics based on parity–time symmetry, Nat. Photonics **11**, 752 (2017).

[5] R. El-Ganainy, K. G. Makris, M. Khajavikhan, Z. H. Musslimani, S. Rotter, and D. N. Christodoulides, Non-Hermitian physics and PT symmetry, Nat. Phys. **14**, 11 (2018).

[6] B. Midya, H. Zhao, and L. Feng, Non-Hermitian photonics promises exceptional topology of light, Nat. Commun. **9**, 2674 (2018).

[7] Y. Ota, K. Takata, T. Ozawa, A. Amo, Z. Jia, B. Kante, M. Notomi, Y. Arakawa, and S. Iwamoto, Active topological photonics, Nanophotonics **9**, 547 (2020).

[8] K. G. Makris, R. El-Ganainy, D. N. Christodoulides, and Z. H. Musslimani, Beam Dynamics in $\mathcal{PT}$ Symmetric Optical Lattices, Phys. Rev. Lett. **100**, 103904 (2008).

[9] A. Guo, G. J. Salamo, D. Duchesne, R. Morandotti, M. Volatier-Ravat, V. Aimez, G. A. Siviloglou, and D. N. Christodoulides, Observation of $\mathscr{P}\mathscr{T}$-Symmetry Breaking in Complex Optical Potentials, Phys. Rev. Lett. **103**, 093902 (2009).

[10] C. E. Rüter, K. G. Makris, R. El-Ganainy, D. N. Christodoulides, M. Segev, and D. Kip, Observation of parity–time symmetry in optics, Nat. Phys. **6**, 192 (2010).

[11] H. Ramezani, T. Kottos, R. El-Ganainy, and D. N. Christodoulides, Unidirectional nonlinear $\mathscr{P}\mathscr{T}$-symmetric optical structures, Phys. Rev. A **82**, 043803 (2010).

[12] Z. Lin, H. Ramezani, T. Eichelkraut, T. Kottos, H. Cao, and D. N. Christodoulides, Unidirectional Invisibility Induced by $\mathcal{PT}$-Symmetric Periodic Structures, Phys. Rev. Lett. **106**, 213901 (2011).

[13] Y. D. Chong, L. Ge, H. Cao, and A. D. Stone, Coherent Perfect Absorbers: Time-Reversed Lasers, Phys. Rev. Lett. **105**, 053901 (2010).

[14] S. Longhi, $\mathscr{P}\mathscr{T}$-symmetric laser absorber, Phys. Rev. A **82**, 031801(R) (2010).

[15] C. Poli, M. Bellec, U. Kuhl, F. Mortessagne, and H. Schomerus, Selective enhancement of topologically induced interface states in a dielectric resonator chain, Nat. Commun. **6**, 6710 (2015).

[16] M. Liertzer, L. Ge, A. Cerjan, A. D. Stone, H. E. Türeci, and S. Rotter, Pump-Induced Exceptional Points in Lasers, Phys. Rev. Lett. **108**, 173901 (2012).

[17] L. Feng, Z. J. Wong, R.-M. Ma, Y. Wang, and X. Zhang, Single-mode laser by parity-time symmetry breaking, Science **346**, 972 (2014).

[18] H. Hodaei, M.-A. Miri, M. Heinrich, D. N. Christodoulides, and M. Khajavikhan, Parity-time symmetric microring lasers, Science **346**, 975 (2014).

[19] B. Peng, Ş. K. Özdemir, S. Rotter, H. Yilmaz, M. Liertzer, F. Monifi, C. M. Bender, F. Nori, and L. Yang, Loss-induced suppression and revival of lasing, Science **346**, 328 (2014).

[20] H. Zhao, P. Miao, M. H. Teimourpour, S. Malzard, R. El-Ganainy, H. Schomerus, and L. Feng, Topological hybrid silicon microlasers, Nat. Commun. **9**, 981 (2018).

[21] M. Parto, S. Wittek, H. Hodaei, G. Harari, M. A. Bandres, J. Ren, M. C. Rechtsman, M. Segev, D. N. Christodoulides, and M. Khajavikhan, Edge-Mode Lasing in 1D Topological Active Arrays, Phys. Rev. Lett. **120**, 113901 (2018).

[22] J. Wiersig, Enhancing the Sensitivity of Frequency and Energy Splitting Detection by using Exceptional Points: Application to Microcavity Sensors for Single-Particle Detection, Phys. Rev. Lett. **112**, 203901 (2014).

[23] W. Chen, Ş. K. Özdemir, G. Zhao, J. Wiersig, and L. Yang, Exceptional points enhance sensing in an optical microcavity, Nature (London) **548**, 192 (2017).

[24] J. Wiersig, Review of exceptional point-based sensors, Photon. Res. **8**, 1457 (2020).

[25] M. V. Berry, Physics of nonhermitian degeneracies, Czech. J. Phys. **54**, 1039 (2004).

[26] M.-A. Miri and A. Alù, Exceptional points in optics and photonics, Science **363**, eaar7709 (2019).

[27] Ş. K. Özdemir, S. Rotter, F. Nori, and L. Yang, Parity–time symmetry and exceptional points in photonics, Nat. Mater. **18**, 783 (2019).

[28] H. Schomerus, Nonreciprocal response theory of non-Hermitian mechanical metamaterials: Response phase transition from the skin effect of zero modes, Phys. Rev. Res. **2**, 013058 (2020).

[29] J. C. Budich and E. J. Bergholtz, Non-Hermitian Topological Sensors, Phys. Rev. Lett. **125**, 180403 (2020).

[30] C. C. Wanjura, M. Brunelli, and A. Nunnenkamp, Topological framework for directional amplification in driven-dissipative cavity arrays, Nat. Commun. **11**, 3149 (2020).

[31] A. McDonald and A. A. Clerk, Exponentially-enhanced quantum sensing with non-Hermitian lattice dynamics, Nat. Commun. **11**, 5382 (2020).

[32] B. Midya, Topological directed amplification, Phys. Rev. A **106**, 053513 (2022).

[33] N. Hatano and D. R. Nelson, Localization Transitions in Non-Hermitian Quantum Mechanics, Phys. Rev. Lett. **77**, 570 (1996).

[34] S. Yao and Z. Wang, Edge States and Topological Invariants of Non-Hermitian Systems, Phys. Rev. Lett. **121**, 086803 (2018).

[35] F. K. Kunst, E. Edvardsson, J. C. Budich, and E. J. Bergholtz, Biorthogonal Bulk-Boundary Correspondence in Non-Hermitian Systems, Phys. Rev. Lett. **121**, 026808 (2018).

[36] C. H. Lee and R. Thomale, Anatomy of skin modes and topology in non-Hermitian systems, Phys. Rev. B **99**, 201103(R) (2019).

[37] D. S. Borgnia, A. J. Kruchkov, and R.-J. Slager, Non-Hermitian Boundary Modes and Topology, Phys. Rev. Lett. **124**, 056802 (2020).

[38] H. Schomerus, Topologically protected midgap states in complex photonic lattices, Opt. Lett. **38**, 1912 (2013).

[39] S. Lieu, Topological symmetry classes for non-Hermitian models and connections to the bosonic Bogoliubov–de Gennes equation, Phys. Rev. B **98**, 115135 (2018).

[40] K. Kawabata, K. Shiozaki, M. Ueda, and M. Sato, Symmetry and Topology in Non-Hermitian Physics, Phys. Rev. X **9**, 041015 (2019).

[41] T. Ozawa, H. M. Price, A. Amo, N. Goldman, M. Hafezi, L. Lu, M. C. Rechtsman, D. Schuster, J. Simon, O. Zilberberg, and I. Carusotto, Topological photonics, Rev. Mod. Phys. **91**, 015006 (2019).

[42] H. Zhou and J. Y. Lee, Periodic table for topological bands with non-Hermitian symmetries, Phys. Rev. B **99**, 235112 (2019).

[43] M. Z. Hasan and C. L. Kane, Colloquium: Topological insulators, Rev. Mod. Phys. **82**, 3045 (2010).

[44] X.-L. Qi and S.-C. Zhang, Topological insulators and superconductors, Rev. Mod. Phys. **83**, 1057 (2011).

[45] C. W. J. Beenakker, Random-matrix theory of Majorana fermions and topological superconductors, Rev. Mod. Phys. **87**, 1037 (2015).

[46] H. Price, Y. Chong, A. Khanikaev, H. Schomerus, L. J. Maczewsky, M. Kremer, M. Heinrich, A. Szameit, O. Zilberberg, Y. Yang, B. Zhang, A. Alù, R. Thomale, I. Carusotto, P. St-Jean, A. Amo, A. Dutt, L. Yuan, S. Fan, X. Yin *et al.*, Roadmap on topological photonics, J. Phys. Photonics **4**, 032501 (2022).

[47] Z. Gong, Y. Ashida, K. Kawabata, K. Takasan, S. Higashikawa, and M. Ueda, Topological Phases of Non-Hermitian Systems, Phys. Rev. X **8**, 031079 (2018).

[48] E. J. Bergholtz, J. C. Budich, and F. K. Kunst, Exceptional topology of non-Hermitian systems, Rev. Mod. Phys. **93**, 015005 (2021).

[49] N. Okuma and M. Sato, Non-Hermitian topological phenomena: A review, arXiv:2205.10379 (2022).

[50] H. Schomerus, Quantum Noise and Self-Sustained Radiation of PT-Symmetric Systems, Phys. Rev. Lett. **104**, 233601 (2010).

[51] G. Yoo, H.-S. Sim, and H. Schomerus, Quantum noise and mode nonorthogonality in non-Hermitian $\mathscr{P}\mathscr{T}$-symmetric optical resonators, Phys. Rev. A **84**, 063833 (2011).

[52] S. Scheel and A. Szameit, $\mathcal{PT}$-symmetric photonic quantum systems with gain and loss do not exist, Europhys. Lett. **122**, 34001 (2018).

[53] M. Brandenbourger, X. Locsin, E. Lerner, and C. Coulais, Non-reciprocal robotic metamaterials, Nat. Commun. **10**, 4608 (2019).

[54] A. Ghatak, M. Brandenbourger, J. van Wezel, and C. Coulais, Observation of non-Hermitian topology and its bulk-edge correspondence in an active mechanical metamaterial, Proc. Natl. Acad. Sci. USA **117**, 29561 (2020).

[55] T. Helbig, T. Hofmann, S. Imhof, M. Abdelghany, T. Kiessling, L. W. Molenkamp, C. H. Lee, A. Szameit, M. Greiter, and R. Thomale, Generalized bulk–boundary correspondence in non-Hermitian topolectrical circuits, Nat. Phys. **16**, 747 (2020).

[56] S. Weidemann, M. Kremer, T. Helbig, T. Hofmann, A. Stegmaier, M. Greiter, R. Thomale, and A. Szameit, Topological funneling of light, Science **368**, 311 (2020).

[57] Q. Liang, D. Xie, Z. Dong, H. Li, H. Li, B. Gadway, W. Yi, and B. Yan, Dynamic Signatures of Non-Hermitian Skin Effect and Topology in Ultracold Atoms, Phys. Rev. Lett. **129**, 070401 (2022).

[58] W. Langbein, No exceptional precision of exceptional-point sensors, Phys. Rev. A **98**, 023805 (2018).

[59] R. Uzdin, A. Mailybaev, and N. Moiseyev, On the observability and asymmetry of adiabatic state flips generated by exceptional points, J. Phys. A: Math. Theor. **44**, 435302 (2011).

[60] J. Doppler, A. A. Mailybaev, J. Böhm, U. Kuhl, A. Girschik, F. Libisch, T. J. Milburn, P. Rabl, N. Moiseyev, and S. Rotter, Dynamically encircling an exceptional point for asymmetric mode switching, Nature (London) **537**, 76 (2016).

[61] J. S. Toll, Causality and the dispersion relation: Logical foundations, Phys. Rev. **104**, 1760 (1956).

[62] R. Keil, C. Poli, M. Heinrich, J. Arkinstall, G. Weihs, H. Schomerus, and A. Szameit, Universal Sign Control of Coupling in Tight-Binding Lattices, Phys. Rev. Lett. **116**, 213901 (2016).

[63] S. Datta, *Electronic transport in mesoscopic systems* (Cambridge University Press, Cambridge, 1997).

[64] T. Guhr, A. Müller-Groeling, and H. A. Weidenmüller, Random-matrix theories in quantum physics: Common concepts, Phys. Rep. **299**, 189 (1998).

[65] U. Kuhl, O. Legrand, and F. Mortessagne, Microwave experiments using open chaotic cavities in the realm of the effective Hamiltonian formalism, Fortschr. Phys. **61**, 404 (2013).

[66] Y. V. Fyodorov and H.-J. Sommers, Statistics of resonance poles, phase shifts and time delays in quantum chaotic scattering: Random matrix approach for systems with broken time-reversal invariance, J. Math. Phys. **38**, 1918 (1997).

[67] E. P. Wigner, Lower limit for the energy derivative of the scattering phase shift, Phys. Rev. **98**, 145 (1955).

[68] F. T. Smith, Lifetime matrix in collision theory, Phys. Rev. **118**, 349 (1960).

[69] V. Gasparian, T. Christen, and M. Büttiker, Partial densities of states, scattering matrices, and Green's functions, Phys. Rev. A **54**, 4022 (1996).

[70] C. Beenakker and P. Brouwer, Distribution of the reflection eigenvalues of a weakly absorbing chaotic cavity, Phys. E **9**, 463 (2001).

[71] J. Wiersig, Nonorthogonality constraints in open quantum and wave systems, Phys. Rev. Res. **1**, 033182 (2019).

[72] T. D. Lee and L. Wolfenstein, Analysis of CP-noninvariant interactions and the $K_1{}^0$, $K_2{}^0$ system, Phys. Rev. **138**, B1490 (1965).

[73] J. S. Bell and J. Steinberger, in *Proceedings of the Oxford International Conference on Elementary Particles*, edited by R. G. Moorhouse, A. E. Taylor, and T. R. Walsh (Oxford University Press, Oxford, 1966).

[74] D. I. Pikulin and Y. V. Nazarov, Two types of topological transitions in finite Majorana wires, Phys. Rev. B **87**, 235421 (2013).

[75] H. Schomerus, From scattering theory to complex wave dynamics in non-Hermitian *PT*-symmetric resonators, Philos. Trans. R. Soc. A **371**, 20120194 (2013).

[76] K. Takata, K. Nozaki, E. Kuramochi, S. Matsuo, K. Takeda, T. Fujii, S. Kita, A. Shinya, and M. Notomi, Observing exceptional point degeneracy of radiation with electrically pumped photonic crystal coupled-nanocavity lasers, Optica **8**, 184 (2021).

[77] A. Hashemi, K. Busch, D. N. Christodoulides, S. K. Ozdemir, and R. El-Ganainy, Linear response theory of open systems with exceptional points, Nat. Commun. **13**, 3281 (2022).

[78] J. Wiersig, Distance between exceptional points and diabolic points and its implication for the response strength of non-Hermitian systems, Phys. Rev. Res. **4**, 033179 (2022).

[79] L. Simonson, S. K. Ozdemir, A. Eisfeld, A. Metelmann, and R. El-Ganainy, Nonuniversality of quantum noise in optical amplifiers operating at exceptional points, Phys. Rev. Res. **4**, 033226 (2022).

[80] C. W. J. Beenakker, Thermal Radiation and Amplified Spontaneous Emission from a Random Medium, Phys. Rev. Lett. **81**, 1829 (1998).

[81] M. Patra, H. Schomerus, and C. W. J. Beenakker, Quantum-limited linewidth of a chaotic laser cavity, Phys. Rev. A **61**, 023810 (2000).

[82] K. Esaki, M. Sato, K. Hasebe, and M. Kohmoto, Edge states and topological phases in non-Hermitian systems, Phys. Rev. B **84**, 205128 (2011).

[83] H. Ramezani, D. N. Christodoulides, V. Kovanis, I. Vitebskiy, and T. Kottos, $\mathscr{P}\mathscr{T}$-Symmetric Talbot Effects, Phys. Rev. Lett. **109**, 033902 (2012).

[84] S. Longhi, D. Gatti, and G. Della Valle, Non-Hermitian transparency and one-way transport in low-dimensional lattices by an imaginary gauge field, Phys. Rev. B **92**, 094204 (2015).

[85] S. Malzard, C. Poli, and H. Schomerus, Topologically Protected Defect States in Open Photonic Systems with Non-Hermitian Charge-Conjugation and Parity-Time Symmetry, Phys. Rev. Lett. **115**, 200402 (2015).

[86] T. E. Lee, Anomalous Edge State in a Non-Hermitian Lattice, Phys. Rev. Lett. **116**, 133903 (2016).

[87] X. Ni, D. Smirnova, A. Poddubny, D. Leykam, Y. Chong, and A. B. Khanikaev, $\mathscr{P}\mathscr{T}$ phase transitions of edge states at $\mathscr{P}\mathscr{T}$

symmetric interfaces in non-Hermitian topological insulators, Phys. Rev. B **98**, 165129 (2018).

[88] F. Mostafavi, C. Yuce, O. S. Maganã-Loaiza, H. Schomerus, and H. Ramezani, Robust localized zero-energy modes from locally embedded $\mathscr{P}\mathscr{T}$-symmetric defects, Phys. Rev. Res. **2**, 032057(R) (2020).

[89] H. Ghaemi-Dizicheh and H. Schomerus, Compatibility of transport effects in non-Hermitian nonreciprocal systems, Phys. Rev. A **104**, 023515 (2021).

[90] K.-I. Imura and Y. Takane, Generalized bulk-edge correspondence for non-Hermitian topological systems, Phys. Rev. B **100**, 165430 (2019).

[91] K. Yokomizo and S. Murakami, Non-Bloch Band Theory of Non-Hermitian Systems, Phys. Rev. Lett. **123**, 066404 (2019).

[92] Z. Yang, K. Zhang, C. Fang, and J. Hu, Non-Hermitian Bulk-Boundary Correspondence and Auxiliary Generalized Brillouin Zone Theory, Phys. Rev. Lett. **125**, 226402 (2020).

[93] W. P. Su, J. R. Schrieffer, and A. J. Heeger, Solitons in Polyacetylene, Phys. Rev. Lett. **42**, 1698 (1979).

[94] M. J. Rice and E. J. Mele, Elementary Excitations of a Linearly Conjugated Diatomic Polymer, Phys. Rev. Lett. **49**, 1455 (1982).